

Human Enhancer of Invasion-Cluster, a Coiled-Coil Protein Required for Passage through Mitosis

Margret B. Einarson,¹ Edna Cukierman,¹ Duane A. Compton,² and Erica A. Golemis^{1*}

Division of Basic Science, Fox Chase Cancer Center, Philadelphia, Pennsylvania 19111,¹ and Department of Biochemistry, Dartmouth Medical School, Hanover, New Hampshire 03755²

Received 13 October 2003/Returned for modification 1 December 2003/Accepted 9 February 2004

In a cross-species overexpression approach, we used the pseudohyphal transition of *Saccharomyces cerevisiae* as a model screening system to identify human genes that regulate cell morphology and the cell cycle. Human enhancer of invasion-cluster (HEI-C), encoding a novel evolutionarily conserved coiled-coil protein, was isolated in a screen for human genes that induce agar invasion in *S. cerevisiae*. In human cells, HEI-C is primarily localized to the spindle during mitosis. Depletion of HEI-C in vivo with short interfering RNAs results in severe mitotic defects. Analysis by immunofluorescence, flow cytometry analysis, and videomicroscopy indicates that HEI-C-depleted cells form metaphase plates with normal timing after G₂/M transition, although in many cases cells have disorganized mitotic spindles. Subsequently, severe defects occur at the metaphase-anaphase transition, characterized by a significant delay at this stage or, more commonly, cellular disintegration accompanied by the display of classic biochemical markers of apoptosis. These mitotic defects occur in spite of the fact that HEI-C-depleted cells retain functional cell cycle checkpoints, as these cells arrest normally following nocodazole or hydroxyurea treatment. These results place HEI-C as a novel regulator of spindle function and integrity during the metaphase-anaphase transition.

In normally dividing human cells, mitosis is regulated by numerous control systems that ensure complete replication and integrity of DNA prior to initiation of the energy-intensive processes of assembly of a mitotic apparatus, chromosome condensation and segregation, and cytokinesis (1, 29, 63). Defects in these processes initiate checkpoints that cause a transient arrest in cell cycle progression to allow repair or trigger apoptosis in cases of irremediable damage (75). Perturbation or loss of such controls on cell division is a common contributing factor to the uncontrolled cell proliferation characteristic of cancer (62, 68). Further, some common cancer therapies, including treatment with antimicrotubule agents, themselves rely on the enhanced susceptibility of some tumor cells to genotoxic stress arising from loss of adequate checkpoint controls (discussed in reference 4). It has been of considerable interest to better understand the mechanisms governing the integrity of progression through the cell cycle.

In mitosis, the activities of the mitotic spindle are critical to drive the physical movements of cellular matter that allow cells to undergo partition. Defects in the formation or function of the mitotic spindle are known to cause abnormal changes in tension at the point of microtubule-kinetochore connection that induce a sensitive spindle checkpoint involving the activation of the BubR1/Bub3/Mad2/Cdc20 protein complex (reviewed in references 5 and 77 and in many other places). In the context of a triggered spindle checkpoint, the anaphase-promoting complex/cyclosome is not activated. As the anaphase-promoting complex/cyclosome has numerous targets in mitosis whose degradation is required for passage beyond prometaphase, including cyclin A (11), and metaphase, including se-

curin (24) and cyclin B (26, 52, 69), depending on the time and source of checkpoint activation and anaphase-promoting complex/cyclosome inhibition, cells with triggered checkpoints may arrest at various points in M phase. Extensive experimentation in many laboratories has shown that spindle checkpoint-induced arrest is protective against cellular death in mitosis.

Some recent studies have begun to analyze the means of coupling between checkpoint activation and antiapoptotic consequences. As one example, depletion of the kinetochore-spindle linker protein hNuf2 leaves intact a spindle checkpoint and causes cell cycle arrest at prometaphase; however, hNuf2-depleted cells are subsequently unable to recover from this arrest and undergo extensive apoptosis (10), suggesting that hNuf2 signals in a critical way to the apoptotic machinery. For this reason, it has been suggested that hNuf2 might be an attractive candidate for the development of a targeted therapeutic agent (10), as its inhibition may provide a means of modulating the protective effect of the spindle checkpoint in some cancer cells.

We were interested in identifying novel human genes that might play a role in these important regulatory functions. To this end, we adapted a cross-species functional complementation strategy. Yeasts have been used for more than a half-century as model organisms to study many cellular processes. Although higher eukaryotic signaling networks are much more complex than those found in *Saccharomyces cerevisiae*, research to date strongly supports the idea that they use similar strategies and components: this conservation of important regulatory factors has permitted the design of powerful high-throughput screens that allow the detection of higher eukaryotic genes with on-signaling pathways of interest, based on their ability to complement or functionally perturb evolutionarily conserved growth control pathways (12, 38, 39). In 1992, Gimeno et al. described the ability of diploid *S. cerevisiae* grown on low-nitrogen medium to convert their budding pat-

* Corresponding author. Mailing address: W406 Fox Chase Cancer Center, 333 Cottman Ave., Philadelphia, PA 19111. Phone: (215) 728-2860. Fax: (215) 728-3616. E-mail: ea_golemis@fccc.edu.

tern from vegetative to pseudohyphal (23). Analysis of the transition from vegetative to pseudohyphal growth in *S. cerevisiae* has subsequently been well established as a useful model for analysis of the coordination of the cell cycle in the context of diverse environmental and internal cues (reviewed in references 33 and 51). Mechanistically, formation of pseudohyphae has been shown to be stimulated by activation of Ras and downstream signaling effectors (23, 44, 58, 60) and, notably, to arise from direct perturbations of proteins that alter cell cycle dynamics (2, 35, 72).

In this study, we provide the initial description of the human enhancer of invasion-cluster (HEI-C) protein, which we isolated based on its ability to induce yeast agar invasion, a characteristic of pseudohyphal growth. HEI-C is a coiled-coil protein with no significant homology to proteins of known function. During mitosis, HEI-C is localized to and biochemically associates with the mitotic spindle. We demonstrate that HEI-C is an essential factor for successful completion of mitosis, as depletion of HEI-C results in mitotic delay and a high frequency of cell death. Cells depleted of HEI-C by transfection of a targeted short interfering RNA (siRNA) manifest a reduced number of cells in the G₂/M compartment (as measured by fluorescence-activated cell sorting [FACS] analysis), concomitant with the appearance of a sub-G₀ peak. Notably, videomicroscopic analysis of synchronized cells depleted of HEI-C demonstrates a high frequency of cellular disintegration or stasis occurring at the metaphase-anaphase transition. Analysis of HEI-C-depleted cells for annexin staining and poly(ADP ribose) polymerase (PARP) cleavage confirms a progressive increase in the percentage of apoptotic cells following HEI-C depletion. HEI-C-depleted cells appear to have normal checkpoint function, as they arrest normally following both hydroxyurea and nocodazole blocks. These and other results indicate that HEI-C provides a novel and critical input into mitosis.

MATERIALS AND METHODS

Yeast screen. A HeLa cell cDNA library constructed in pJG4-4 (*TRP1*⁺; cDNAs inducibly expressed under the control of the *GAL1* promoter; library gift of J. Gyuris) was transformed into the *S. cerevisiae* strain CGx74 (*MATα/a trp1/trp1*; gift of C. Gimeno), a diploid strain derived from the parent strain Σ1278b (23, 45). Cells were plated at a density of approximately 60,000 cells per 10-cm plate of complete minimal medium lacking tryptophan and with 2% galactose. Plates were maintained at 30°C for approximately 60 h and subsequently washed with vigorous blasts of distilled water. Highly invasive patches observed on plates lacking tryptophan with galactose were cored with the narrow end of a Pasteur pipette and transferred to plates lacking tryptophan and with 2% glucose. These colonies were streaked to single colonies on fresh plates lacking tryptophan and with glucose and reassayed for the invasive phenotype on plates lacking tryptophan and with galactose.

Plasmid DNA was isolated from invasive colonies, retransformed into naïve CGX74, and reassayed for enhancement of filamentation and agar invasion versus the vector JG4-4 on plates lacking tryptophan and with galactose and on SLAGR (low-nitrogen medium with 2% galactose and 1% raffinose [23]). The cDNAs were restriction mapped and sequenced. 5' rapid amplification of cDNA ends was performed with the GENERACER kit (Invitrogen, Carlsbad, Calif.); total RNA from HeLa cells was isolated and used as the substrate with HEI-C probes centered around the first coding ATG. The products were cloned and sequenced. The longest clone of HEI-C obtained in the pseudohyphal screen was 1,097 bp, including 834 bp of putative coding sequence. Exhaustive 5'-rapid amplification of cDNA end PCR on HeLa total RNA led to identification of 14 bp of additional 5' sequence containing an in-frame stop codon, confirming isolation of the full-length coding sequence for HEI-C within the original clone identified in the agar invasion screen.

Filamentation and agar invasion assays. CGX74 and CG188, isogenic diploid and haploid strains, respectively, were transformed with the indicated clones. To assay for invasion, transformants were replica plated on plates lacking tryptophan and uracil with glucose or lacking tryptophan and uracil and with galactose and raffinose and incubated at 30°C for 24 h. Plates were photographed prior to washing, subsequently washed with several blasts of distilled water, and rephotographed. To assay for filamentation, transformants were streaked onto SLAGR medium which had been freshly poured onto sterilized glass slides. After 24 h at 30°C colony images were captured at 20× on a Nikon microscope with a charge-coupled device camera.

Plasmids. All clones obtained from the screen are in the yeast galactose-inducible vector pJG4-4. Four clones of HEI-C were isolated, including three identical long clones designated HEI 8, HEI 15, and HEI 21 (encoding amino acids 1 to 278), and one truncated clone designated HEI 22 (amino acids 77 to 278). Three clones of PRK2 were isolated, encompassing the C-terminal region of the protein, including the kinase domain, HEI 16 (amino acids 505 to 984), HEI 7, and HEI 14 (amino acids 577 to 984). The HEF1 clone obtained in the screen (HEI 11) comprises the C-terminal domain of HEF1 (amino acids 660 to 834), similar to the previously described clone HEF1-C (34). The HEI 15 clone (nucleotides +1 to 837 of HEI-C, encoding amino acids 1 to 278) was first cloned into pUC119 by PCR to generate a cDNA with a 5' MunI site and a 3' XhoI site. This insert was subcloned into pcDNA3 to make pcDNA3/HEI-C. Note that HEI-C has been assigned the official symbol CCDC5 by the International Radiation Hybrid Mapping Consortium.

Antibodies. An antipeptide antibody to the carboxy-terminal 16 amino acids of HEI-C (amino acid sequence SSIEAELTRRVDMML) was generated. The peptide was conjugated to keyhole limpet hemocyanin and used as an immunogen to produce polyclonal rabbit antiserum (Research Genetics, Inc., Huntsville, Ala.). HEI-C antibodies were affinity purified with the 16-mer peptide as previously described (34). For Western and immunofluorescence analysis, anti-HEI-C antibodies were used at a 1:100 dilution. Monoclonal anti-α-tubulin antibodies (clone DM1A; Sigma, St. Louis, Mo.) were used at a 1:2,000 dilution for immunofluorescence. E-cadherin antibodies (BD Transduction Labs, San Diego, Calif.) were used at a 1:100 dilution for immunofluorescence. Antibodies to gamma-tubulin were from Sigma. Two anti-PARP antibodies were used, p85-PARP (Promega, Madison, Wis.) and anti-PARP (Calbiochem, San Diego, Calif.). Dichlorotriazinyl-amino-fluorescein goat anti-mouse immunoglobulin (Jackson Immunological Laboratories, West Grove, Pa.) and rhodamine-X goat anti-rabbit immunoglobulin (Molecular Probes, Eugene, Ore.) secondary antibodies were used at 1:500 for immunofluorescence. For Western blotting, secondary horseradish peroxidase-conjugated sheep anti-rabbit immunoglobulin antibody (Amersham, Piscataway, N.J.) was used at a dilution of 1:4,000.

Cell culture. MCF7 (human epithelium-like breast adenocarcinoma), HeLa (human epithelial adenocarcinoma), U2OS (human osteosarcoma) cells, and COS7 (simian virus 40-transformed African Green monkey kidney) cells were maintained in Dulbecco's modified Eagle's medium plus 10% fetal bovine serum supplemented with penicillin and streptomycin. MDCK (canine kidney epithelial, clone 8; gift of W. J. Nelson) cells were maintained in Dulbecco's modified Eagle's medium, low glucose, supplemented with 10% fetal bovine serum. For cell synchronization, cells were blocked with nocodazole by treatment with 1 μM nocodazole for 15 h. Cells were harvested by mitotic shake off, washed, and lysed or fixed for immunofluorescence (see below). For cell synchronization, double thymidine block, nocodazole arrest, and hydroxyurea treatment were evaluated; the last was consistently the least toxic and most effective. Cells treated with hydroxyurea were treated with 2 mM hydroxyurea for 20 h. After 20 h, cells were either harvested (see below) or washed twice with medium minus drug and released into the cell cycle.

siRNA transfection. siRNA oligonucleotides were designed according to the manufacturer's guidelines (www.dharmacon.com). RNA oligonucleotides HEI-C.A (AAGGAUACCUCGCUAGCUAGU) or a scrambled oligonucleotide control were transfected with Oligofectamine (Invitrogen) according to the manufacturer's instructions. For immunofluorescence, coverslips in six-well dishes were transfected with 80 pmol of RNA duplex per well. For FACS analysis, cells were plated in a 10-cm dish and transfected with 150 pmol of RNA duplex. Cells were processed for analysis 24 h after transfection. The degree of depletion of HEI-C was measured by use of NIH Image to quantitate scanned images of Western blots with HEI-C-specific antibodies, with protein levels normalized by analysis of actin controls.

Northern analysis. An oligonucleotide probe based on the HEI-C coding sequence (5' TTT TAG AAA GTC CAT GTT CTG ACG ACG 3') was 5'-end labeled and used to probe a multitissue Northern blot containing polyadenylated mRNA (Clontech, Palo Alto, Calif.).

Western analysis. Cells were lysed in radioimmunoprecipitation assay (RIPA) buffer supplemented with protease and phosphatase inhibitors (150 mM NaCl,

50 mM Tris [pH 8.0], 1% IGEPAL, 0.5% deoxycholate, 0.1% sodium dodecyl sulfate [SDS], 0.1 mg of aprotinin per ml, 0.1 mg of leupeptin per ml, and 1 mM orthovanadate). Analysis of proteins by Western blotting was performed by standard methodology. Results of Western analysis were visualized with chemoluminescence (New England Nuclear, Boston, Mass.).

Immunofluorescence. Three different fixation-permeabilization protocols were followed; unless otherwise indicated, all manipulations were carried out at room temperature. For paraformaldehyde fixation, cells on coverslips were washed with phosphate-buffered saline (PBS) and then incubated in 4% paraformaldehyde prepared in PBS (pH 7.2) for 10 min. The cells were permeabilized in PBS containing 0.2% Triton X-100 for 5 min. The cells were next washed with PBS plus 0.2% bovine serum albumin and incubated with the indicated antibody in PBS plus 0.2% bovine serum albumin for 1 h. The coverslips were then washed three times in excess PBS plus 0.2% bovine serum albumin, and secondary antibodies were added at the indicated concentrations for 1 h. The coverslips were washed as before and mounted with Vectashield mounting medium (Vector Labs, Burlingame, Calif.). For preextraction and methanol fixation, samples were preextracted by a method similar to that of O'Connell and Wang (53) by incubation in PHEM buffer containing 100 mM PIPES piperazine-*N,N'*-bis(2-ethanesulfonic acid) (PIPES, pH 6.9), 25 mM HEPES (pH 6.9), 1 mM EGTA, and 2 mM MgSO₄ plus 0.02% Triton X-100 and 5 μ M paclitaxel (Sigma) for 1 min. The cells were subsequently fixed in methanol at -20°C for 5 min prior to incubation with antibodies as described above. For the -20°C methanol fixation, coverslips were incubated in methanol at -20°C for 10 min and incubated with antibodies as described above. Images of cells were captured with a spinning-disk confocal scanning head (Perkin-Elmer, Wellesley, Mass.) equipped with a triple laser for multichannel fluorescent acquisition mounted on an Eclipse TE2000-S inverted microscope (Nikon). Images were further configured with Adobe Photoshop 7.0 software.

Microtubule pulldown. Microtubules were polymerized from purified tubulin (Molecular Probes) by incubation in G-PEM buffer (100 mM PIPES [pH 6.8], 1 mM EGTA, 1 mM MgSO₄, 1 mM GTP, and 30% glycerol) at 37°C for 10 min and with a subsequent addition of paclitaxel (Sigma) to a final concentration of 10 μ M. HeLa cells were lysed by Dounce homogenization in PHEM buffer plus 0.1 mg of aprotinin per ml, 0.1 mg of leupeptin per ml, and 1 mM orthovanadate. The cell lysate was precleared by centrifugation at $52,000 \times g$ for 1 h at 4°C . The supernatant was incubated for 30 min at 37°C with 5 μ g of polymerized microtubules. The reactions were layered on a 15% sucrose solution in PB buffer (80 mM PIPES [pH 6.9], 1 mM EGTA, 1 mM CaCl₂) and centrifuged at $30,000 \times g$ for 30 min at room temperature. Pellets were resuspended in PHEM buffer and stored with their supernatants at -20°C until use.

Preparation and immunodepletion of mitotic extracts. Mitotic extracts from HeLa cells were prepared according to Gaglio et al. (19). HeLa cells were synchronized in the cell cycle by double block with 2 mM thymidine. Following release from thymidine block, the cells were allowed to grow for 6 h, and then nocodazole was added to a final concentration of 40 ng/ml. The mitotic cells that accumulated over the next 4 h were collected by mitotic shake off and incubated for 30 min at 37°C with 20 μ g of cytochalasin B per ml. The cells were then collected by centrifugation at 1,500 rpm and washed twice with cold PBS containing 20 μ g of cytochalasin B per ml. Cells were washed one last time in cold KHM buffer containing 20 μ g of cytochalasin B per ml and finally Dounce homogenized (tight pestle) at a concentration of $\approx 3 \times 10^7$ cells/ml in KHM buffer containing 20 μ g of cytochalasin B per ml, 20 μ g of phenylmethylsulfonyl fluoride per ml, and 1 μ g each of chymostatin, leupeptin, antipain, and pepstatin per ml. The crude cell extract was then subjected to sedimentation at $100,000 \times g$ for 15 min at 4°C . The supernatant was recovered and supplemented with 2.5 mM ATP (prepared as Mg²⁺ salts in KHM buffer) and 10 μ M taxol, and assembly of mitotic asters was induced by incubation at 30°C for 30 to 60 min. Samples were processed for immunofluorescence as previously described (19). The remainder of the extract containing the assembled mitotic asters was sedimented at $10,000 \times g$ for 15 min at 4°C . The supernatant and pellet fractions were recovered and solubilized in sodium dodecyl sulfate-polyacrylamide gel electrophoresis (SDS-PAGE) sample buffer for immunoblot analysis.

Immunodepletion of the extract prior to aster assembly was carried out with ≈ 50 μ g of either HEI-C affinity-purified antibodies or preimmune rabbit immunoglobulin G. Each antibody was adsorbed onto 25 μ l of protein A-conjugated agarose (Boehringer Mannheim, Indianapolis, Ind.). The antibody-coupled agarose was washed in KHM buffer and then packed by centrifugation to remove the excess fluid. Half the antibody-coupled agarose was resuspended with the mitotic extract and incubated with agitation for 1 h at 4°C . Following this incubation, the agarose was removed from the extract by sedimentation at $15,000 \times g$ for 10 s and saved. Next, the extract was recovered and used to resuspend the other half of the antibody-coupled agarose, and another incubation was performed with

agitation for 1 h at 4°C . Following this incubation, the agarose was removed by sedimentation at $15,000 \times g$ for 10 s and pooled with the agarose pellet from the initial depletion reaction. The depleted extract was recovered, and microtubule polymerization was induced by the addition of taxol and ATP and incubation at 30°C for 30 to 60 min.

Video microscopy. Cells were blocked in hydroxyurea as described above and released into drug-free medium. Cells were observed with a TE 2000-S inverted microscope (Nikon) equipped with a homemade environmental stage controlling temperature, humidity, and CO₂ levels and a Photometrics Quantix cooled charge-coupled device camera. Phase contrast images were obtained at 4-min intervals for 24 to 48 h after release from cells transfected with a control siRNA or the HEI-C siRNA (see above), and processed with ISEE Invision software. The movies were analyzed with Quicktime and Excel software.

FACS analysis. Samples were harvested by combining the floating cells in the culture medium with the adherent cells detached with trypsin-EDTA, and this cell suspension was subsequently centrifuged at 1,500 rpm for 5 min at 4°C . Cells to be stained with propidium iodide were fixed in -20°C 70% ethanol overnight prior to staining. Cells were then washed twice with ice-cold PBS and centrifuged at 1,500 rpm for 5 min at 4°C . Cell pellets were resuspended in 500 μ l of propidium iodide stain (38 mM sodium citrate, 50 μ g of propidium iodide per ml, 20 μ g of RNase A per ml) and incubated for 30 min at 37°C in the dark. Live-cell annexin and propidium iodide staining was accomplished with the Apo-Alert annexin V-EGFP apoptosis kit (BD-Clontech, Palo Alto, Calif.), as per the manufacturer's instructions. A Becton Dickinson FACScan coupled with CellQuest software was used to obtain FACS data. The FACS data were subsequently analyzed with FlowJo software (TreeStar, Ashland, Ore.).

RESULTS

Isolation of HEI-C. A screen of 500,000 primary transformants of a human HeLa cDNA expression library to identify proteins inducing agar invasion yielded 14 independent clones that reproducibly generated an invasive phenotype (see Materials and Methods for details). Some of the novel cDNAs, encoding HEF1 (15, 37–37, 54, 55) and HEI10 (71), we have now characterized as regulators of cell attachment and cell division. Of the remaining cDNAs, three independent clones were activating truncations of PRK2 (57), a serine-threonine kinase which has been shown to be stimulated by activated Rho and Rac and is involved in the regulation of the actin cytoskeleton (3, 16, 59, 74). However, the most abundant class of clones obtained in the screen included four independent clones of a novel cDNA sequence we have termed human enhancer of invasion-cluster, or HEI-C, to reflect its frequency of isolation.

Pseudohyphal growth in *S. cerevisiae* can be induced through stimulation of multiple distinct signaling pathways, including modulation of the STE mitogen-activated protein kinase cascade (as with HEF1), direct modulation of cell cycle compartmentalization (as with HEI10), or through alternative mechanisms, as reviewed in reference 61. We comparatively analyzed the effect of the HEF1, HEI-C, and PRK2 isolates on induction of agar invasion and pseudohyphal growth. The clones of HEI-C, HEF1, and PRK2 isolated in the screen induced agar invasion on rich medium (Fig. 1A) and enhanced filamentation on low-nitrogen medium in diploids (Fig. 1B). However, PRK2 and HEI-C additionally enhanced invasiveness on rich medium and filamentation on low-nitrogen medium in haploids, while the HEF1 did not (Fig. 1A and B). This result suggested that PRK2 and HEI-C are likely to be mediating these phenotypes through activation of different pathways than HEF1. As the PRK2 protein has already been well studied, we focused further efforts on HEI-C.

HEI-C gene and protein structure. The completed HEI-C cDNA sequence is identical to that described in GenBank for

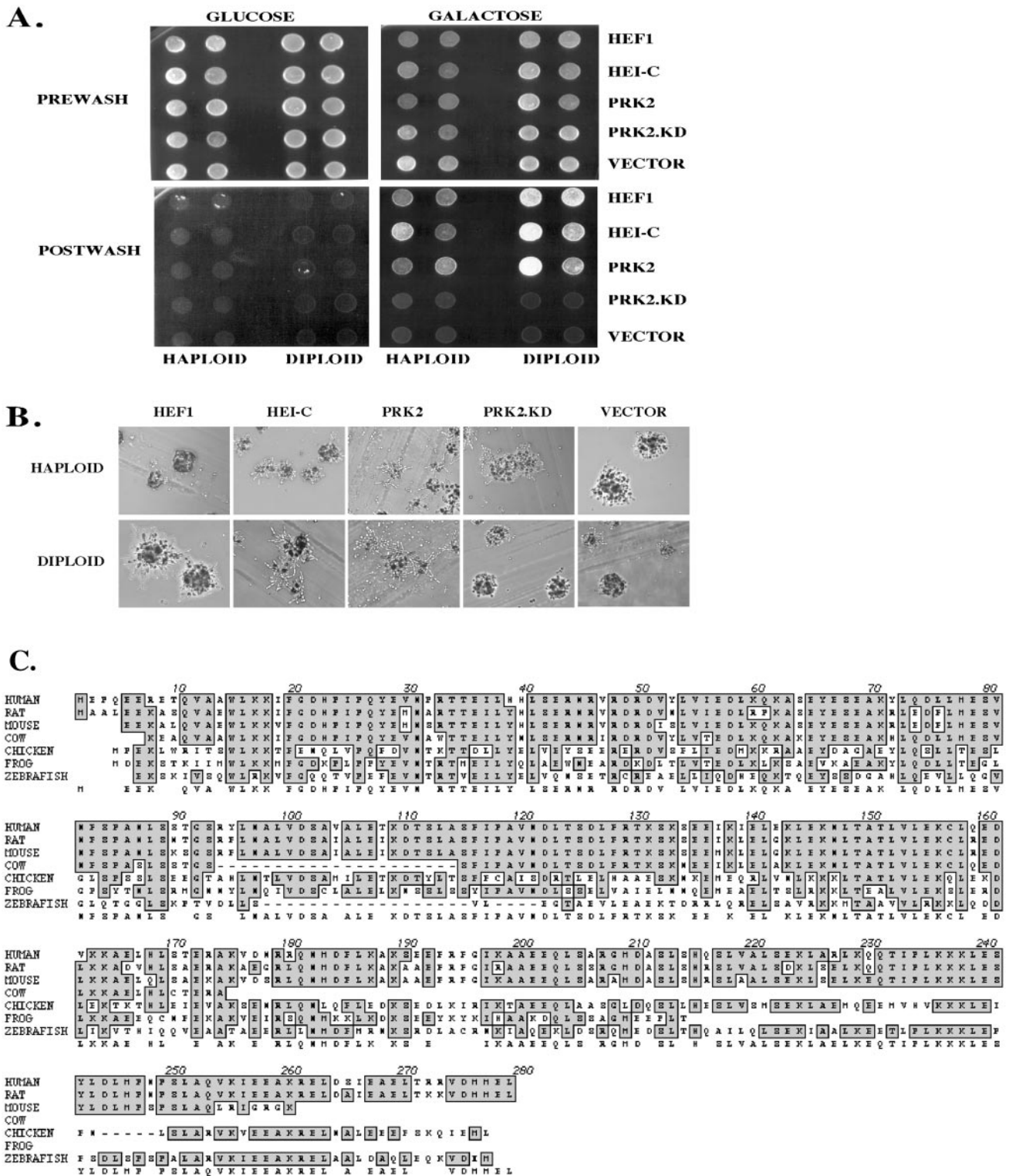


FIG. 1. HEI-C causes invasive and filamentous growth in *S. cerevisiae*. (A) Assay for invasive growth. Diploid CGx75 or isogenic haploid CG188 *S. cerevisiae* strains were transformed with plasmids isolated in the library screen expressing HEF1 (amino acids 660 to 834), PRK2 (amino acids 505 to 984), a kinase dead mutant of the PRK2 clone (PRK2-KD) or HEI-C (amino acids 1 to 278, full-length), and two independent transformants replica plated onto plates lacking uracil and tryptophan and with glucose (gene expression off) or lacking uracil and tryptophan and with galactose (gene expression on). After 24 h of growth, the plates were photographed (prewash), washed with running distilled water, and rephotographed (postwash). (B) Assay of filamentous growth. Diploid CGx75 or isogenic haploid CG188 *S. cerevisiae* strains were transformed with the HEF1, PRK2, PRK2.KD, or HEI-C clones isolated in the invasive screen and streaked onto SLAGR low-nitrogen medium poured on glass slides. After 24 h of growth, the filamentous phenotype was recorded. (C) Comparison of human HEI-C to rat HEI-C and of protein sequences translated from a compiled mouse EST clone, a bovine EST, a compiled chicken EST, a frog EST, and a compiled zebra fish EST demonstrates sequence homology. Identical residues are shaded and boxed; the bottom line of the sequence is the consensus.

hypothetical protein BC014003, at locus ID 115106, and is 1,118 bp, encoding a predicted protein of 278 amino acids. Based on the currently compiled human genome sequence, the *HEI-C* gene is encoded by 10 exons and is located at chromosome 18q21.1. Three pseudogenes for *HEI-C* exist on chromosomes 5, 8, and X. Comparison of the predicted coding sequence of *HEI-C* to sequences from putative orthologs found in multiple chordate and plant sequences in GenBank indicates a conserved protein structure (Fig. 1C), in which the Coils2 program (46) identified three potential coiled-coil domains (coil 1, amino acids 49 to 79; coil 2, amino acids 124 to 177; coil 3, amino acids 249 to 278). In addition, a putative nuclear exclusion sequence (28, 49) is present in the C terminus of the protein and well conserved among *HEI-C* orthologs (amino acids 234 to 244). The leucine-rich nuclear exclusion sequence was first identified in the signal transduction protein PKI and the human immunodeficiency virus protein Rev (28, 49, 76), and proteins containing this sequence have been shown to be exported from the nucleus by a CRM1-dependent mechanism (17, 66). The overall homology between the predicted *HEI-C* orthologs and the human protein is typical for human versus rodent comparisons (for example, mouse, 84% identity and 88% similarity), based on known conservation frequencies (48). A similarly high conservation is observed with other chordates (cow, 89% identity and 92% similarity; frog, 54% identity and 62% similarity). No proteins closely related to *HEI-C* at the level of primary sequence exist in *Drosophila melanogaster*, *Caenorhabditis elegans*, or yeasts.

HEI-C is abundantly expressed in mammalian cells. The *HEI-C* mRNA is readily detectable in multiple human tissues by Northern analysis of polyadenylated mRNA (Fig. 2A). A single transcript of approximately 1.2 to 1.3 kb was detected in all tissues tested and was most abundant in pancreas, heart, liver, kidney, and muscle. Supporting this indication of abundance, the *HEI-C* transcript is well represented among expressed sequence tag (ESTs) in GenBank derived from sequencing of libraries prepared from many different tissue sources (results not shown). Affinity-purified antibodies generated to a peptide encoding the 16 carboxy-terminal amino acids of *HEI-C*, conserved in *HEI-C* from multiple species, reacted with a single polypeptide of approximately 32 kDa in HeLa, MDCK, COS7, and MCF7 cells (Fig. 2B). In mammalian and *S. cerevisiae* cells overexpressing *HEI-C*, the protein product of the isolated cDNA comigrated with this endogenous species (Fig. 2C), confirming that the expressed *HEI-C* cDNA encompasses the complete coding region of the gene.

HEI-C associates with the mitotic spindle. To begin to elucidate the normal function of *HEI-C*, we used the anti-*HEI-C* antibody in immunofluorescence studies of HeLa, MCF7, and MDCK cells throughout cell cycle. The most distinctive feature of *HEI-C* localization was its prominent association with the spindle poles in mitotic cells (Fig. 3A). In metaphase (Fig. 3A, panel a), *HEI-C* is localized to the mitotic asters and is highly punctate on the microtubule array. During later stages of mitosis, *HEI-C* remains on the spindle but is not present at the interzone (Fig. 3A, panel b), and finally *HEI-C* is observed at the microtubule bundles proximal to the midbody, clearly excluded from the midbody (Fig. 3A, panel c).

Confocal analysis of HeLa cells costained for *HEI-C* and α -tubulin (Fig. 3B) shows colocalization with tubulin at the

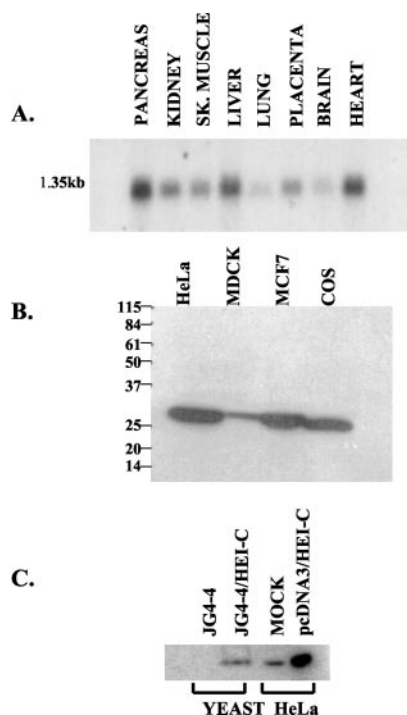


FIG. 2. Expression of *HEI-C* mRNA and protein. (A) A multiple-tissue Northern blot was probed with a 32 P-labeled *HEI-C* oligonucleotide probe. A single message of approximately 1.3 kb was detected. (B) Western analysis of 10 μ g of total-cell lysates from HeLa, MDCK, MCF7, and COS7 cells. Cells were lysed in RIPA buffer, subjected to electrophoresis on an SDS-10% PAGE gel, transferred to a polyvinylidene difluoride membrane, and immunoblotted with affinity-purified rabbit polyclonal anti-peptide *HEI-C* antibodies. (C) Expression of the *HEI-C* clone in *S. cerevisiae* and mammalian cells produces a protein that comigrates with endogenous *HEI-C*. Total-cell lysate isolated from CGx75 transformed with vector alone (lane 1) or *HEI-15* (lane 2) and grown in galactose and total-cell lysate from mock-transfected HeLa cells (lane 3) or HeLa cells transfected with *HEI-C* (lane 4) were subjected to electrophoresis on an SDS-10% PAGE gel, transferred to a polyvinylidene difluoride membrane, and probed with affinity-purified anti-peptide *HEI-C* antibodies.

spindle poles as well as along the microtubule array, extending towards the chromosomes in mitotic cells. *HEI-C* localization to the spindle poles in mitosis may emanate from an initial localization to the centrosome, as in interphase cells *HEI-C* is at the centrosome, as demonstrated by costaining with γ -tubulin (Fig. 3C), with the remainder of the protein diffuse in the cytoplasm. Of further interest, in MCF7 and MDCK cells, *HEI-C* localized to regions of cell-cell contact in some but not all cells (Fig. 3D). The significance of this cell junctional staining is not yet understood but may indicate that *HEI-C* is involved in communications between the cell attachment and cell divisional machinery.

In contrast to the results in mitotic cells, *HEI-C* does not notably colocalize with the tubulin cytoskeleton in interphase cells (data not shown). The differences in *HEI-C* association with microtubules in interphase versus M-phase cells could derive from the contribution of cell cycle-regulated posttranslational modifications of *HEI-C* or changes in the gross levels of *HEI-C*. Lysates were prepared from cells synchronized by double thymidine block and then harvested at different times

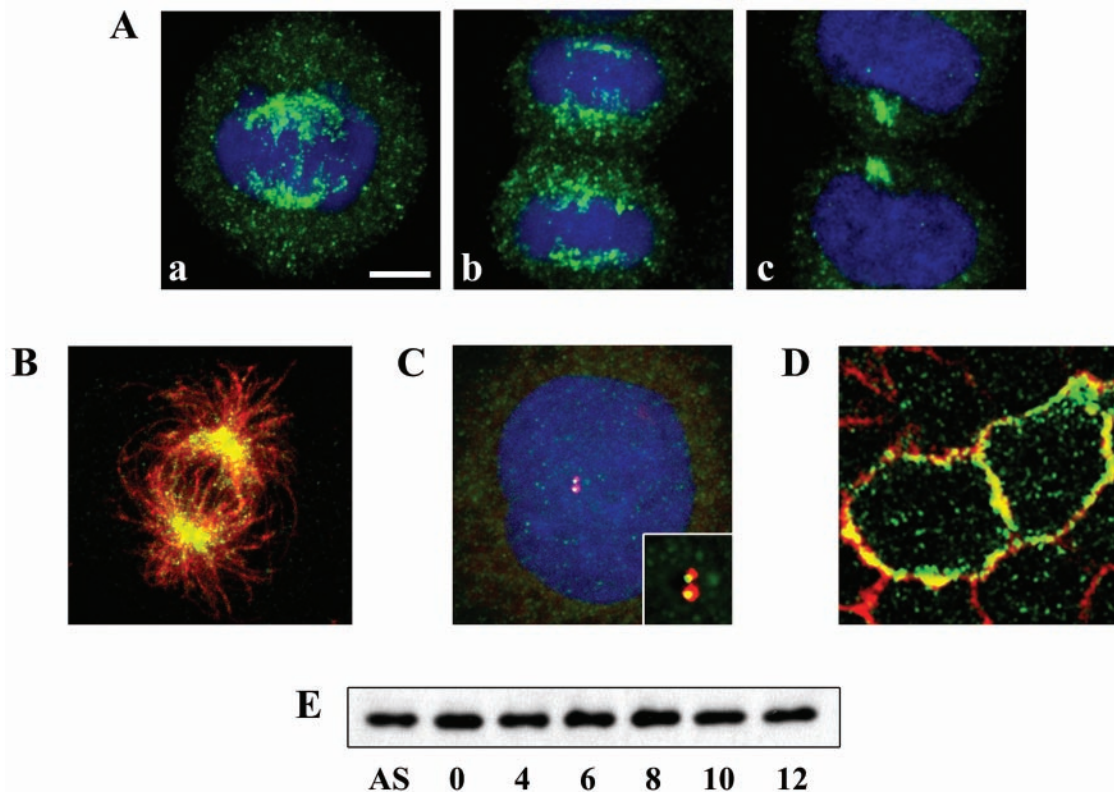


FIG. 3. HEI-C localizes to the spindle during mitosis. (A) MCF7 cells were initially synchronized with nocodazole, released, and allowed to progress through mitosis. HEI-C is shown in green. DNA was labeled with propidium iodide and digitally assigned to be blue. Bar, 5 μ m. (B) Confocal analysis of unsynchronized cells double-labeled for HEI-C (in green) and α -tubulin (in red). (C) Interphase MCF7 cells labeled to visualize HEI-C (green), γ -tubulin (red), or DNA (blue). The inset shows a zoomed yellow colocalization of HEI-C and γ -tubulin only (e.g., in the absence of the blue channel). (D) MDCK cells were stained with antibody to HEI-C (green) or to E-cadherin (red) to demonstrate HEI-C localization to cell junctions. (E) Western blot analysis of HeLa cells synchronized by double thymidine block (time zero), released, then harvested at 4, 6, 8, 10, or 12 h, as indicated, and compared with asynchronous cells (AS). Lysates were subjected to electrophoresis on an SDS-10% PAGE gel, transferred to a polyvinylidene difluoride membrane, and probed with affinity-purified anti-peptide HEI-C antibodies.

following release. Western analysis demonstrated that HEI-C levels are constant through the cell cycle, and the protein does not have obvious cell cycle-regulated changes in gel mobility suggestive of phosphorylation or other modifications (Fig. 3E).

To further explore the association of HEI-C with microtubules, an *in vitro* microtubule pulldown assay was used (51). Extracts prepared from asynchronously growing HeLa cells were incubated with purified, polymerized microtubules. These reactions were then layered onto a sucrose cushion and centrifuged to separate the polymerized microtubules and associated proteins recovered in the pellet from the remainder of the lysate (Fig. 4A). In the absence of microtubules, most of the HEI-C partitioned to the supernatant, but in the presence of polymerized microtubules, an increased fraction of HEI-C was recovered in the pellet (22%, versus 5% without microtubules). No HEI-C was obtained in pellet fractions in the absence of taxol (data not shown). This indicates that endogenous HEI-C from asynchronous (i.e., predominantly interphase) cells is competent to associate with polymerized microtubules *in vitro*.

Based on the immunofluorescence data above, showing HEI-C association with the mitotic spindle, we suspected that the low efficiency of microtubule binding was due to the large

percentage of nonmitotic cells in the asynchronous cell population used to make lysates for this assay. To address this possibility, we prepared mitotic extracts from synchronized cells and induced the polymerization of microtubules from endogenous pools of tubulin with taxol under conditions that lead to microtubule organization into asters (9, 19). Organization of microtubules into asters under these conditions is cell cycle dependent and centrosome independent and requires dynein, dynactin, Eg5, HSET, and NuMA (8) (see Materials and Methods). Western analysis of the pellet and supernatant fractions from synchronized HeLa cells showed recruitment of approximately 63% of HEI-C to the aster-containing pellet fraction (Fig. 4B). These data demonstrate that the efficiency with which HEI-C associates with microtubules increases in mitosis, consistent with the HEI-C localization determined by immunofluorescence analysis. Unfortunately, recombinant HEI-C expressed in bacteria aggregates and pellets in the absence of microtubules, impeding our ability to test if HEI-C interacts with microtubules directly.

The mitosis-specific increase in microtubule binding efficiency suggested that HEI-C might associate with other proteins to facilitate its association with microtubules. To test this idea, we analyzed the distribution of HEI-C in HeLa mitotic

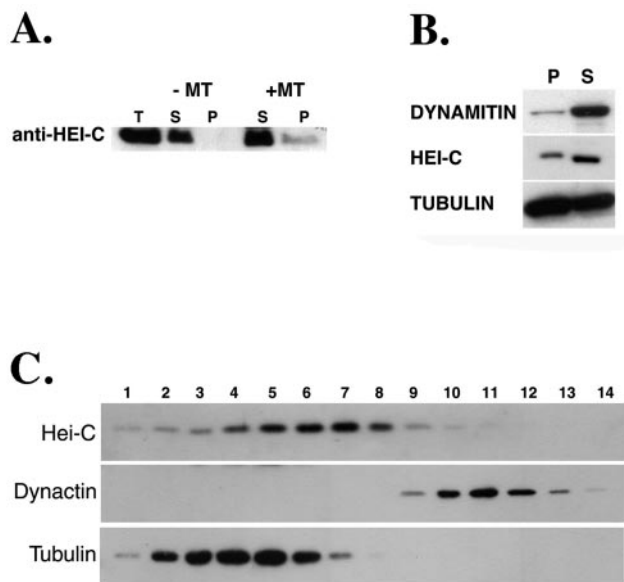


FIG. 4. HEI-C is associated in vitro with mitotic asters. (A) HeLa cells were lysed by Dounce homogenization in PHEM buffer, and the cell lysate was precleared by centrifugation. The supernatant was incubated either with (+MT) or without (-MT) microtubules that had been previously polymerized from purified tubulin by incubation in G-PEM buffer. The reactions were layered on a 15% sucrose solution and centrifuged. Total-cell lysate (T) or the resulting supernatant (S) or pellet (P) fractions were subjected to SDS-PAGE, and proteins were subsequently transferred to polyvinylidene difluoride and immunoblotted with affinity-purified anti-HEI-C antibodies. Quantitation was done with NIH Image analysis of scanned films. (B) Taxol and ATP were added to HeLa cell mitotic extracts to stimulate aster formation. Asters were pelleted, and the insoluble (P) and soluble (S) fractions were subjected to electrophoresis and immunoblotting with the indicated antibodies and quantitation as in A. (C) A HeLa cell mitotic extract was fractionated on a 5 to 20% sucrose gradient, and fractions ranging from the top (no. 1) to bottom (no. 14) were collected. Western analysis of these fractions was performed with antibodies specific for HEI-C, dynactin, and tubulin, as indicated.

extracts that were sedimented through a sucrose gradient. The distribution of HEI-C versus two reference proteins, tubulin and dynactin, was determined by Western blot analysis (Fig. 4C). Tubulin is a heterodimer of α and β subunits with a sedimentation coefficient of 6S. Dynactin is a large multisubunit complex with a sedimentation coefficient of 20S. HEI-C showed a broad distribution in these gradients, with a peak at approximately 10S. This sedimentation profile indicates that HEI-C exists at mitosis in a protein complex with a molecular mass much larger than expected based on its amino acid sequence. At present we do not know if that complex is homo- or hetero-oligomeric, but the result suggests that HEI-C association with other proteins may contribute to its mitotic localization profile.

HEI-C depletion decreases the G_2/M cell cycle compartment and induces apoptosis. To address the function of HEI-C at the spindle, we compared HeLa cells that were transfected with an siRNA duplex (14) designed to target HEI-C (HEI-C.A) or transfected with an irrelevant siRNA (Luciferase or scrambled sequence) or mock transfected or untreated. The HEI-C-specific siRNA duplex efficiently depleted HEI-C (Fig.

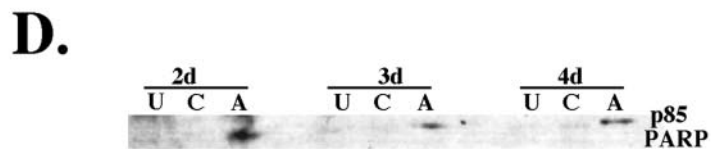
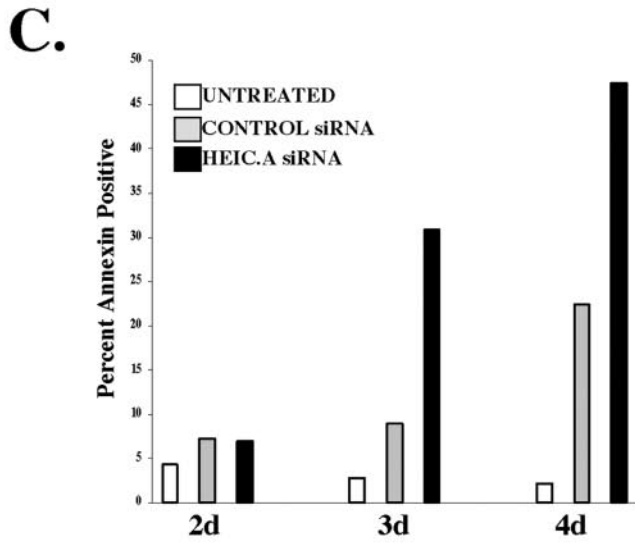
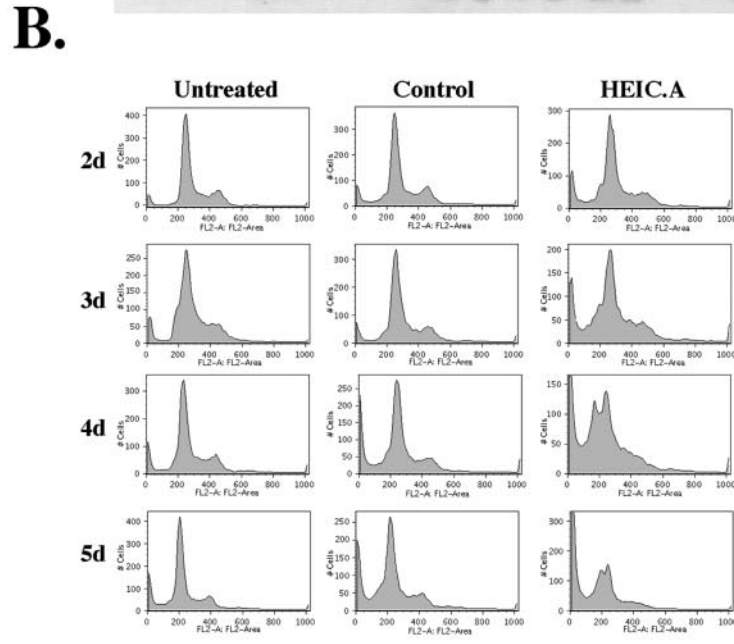
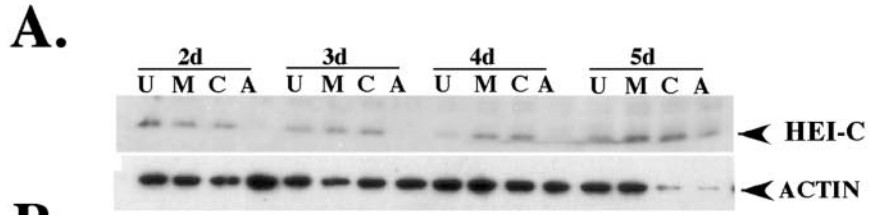
5A). HEI-C protein levels were noticeably reduced by 24 h (not shown) following transfection and 75% depleted by 2 days and remained depleted for at least 5 days. Based on quantitation of images, HEI-C levels were consistently reduced by 80 to 90% at 72 to 96 h post-siRNA treatment.

An initial characterization of the cell cycle profile of HEI-C-depleted cells was performed by propidium iodide staining and FACS analysis (Fig. 5B). In HEI-C-depleted cells, one striking change in the cell cycle profile was the appearance of a large sub- G_0 peak as the cells remained in culture posttransfection with HEI-C-directed siRNA. The sub- G_0 peak was evident by 2 days of HEI-C depletion (7.2%) and increased thereafter. In addition, the G_2/M compartment of the cell cycle was reduced relative to controls at day 4 following depletion, while debris accounted for 21.9% and the sub- G_0 peak accounted for 28.3% of the total propidium iodide-stained sample. Our routine observation of cells depleted of HEI-C showed significant reductions in cell number versus mock-transfected cells, and upon staining of these cells with 4',6'-diamidino-2-phenylindole (DAPI), large numbers of fragmented nuclei were observed (data not shown).

Together, these observations suggested that HEI-C-depleted cells might be undergoing apoptosis (7). To confirm this interpretation, HEI-C-depleted cells were assayed (Fig. 5C and 5D) by live-cell annexin and propidium iodide costaining, as well as by PARP cleavage. Annexin staining of HEI-C-depleted cells on days 2, 3, and 4 posttransfection showed an increase in annexin-positive cells in HEI-C-depleted cells on day 3 (30.7%) versus control transfected cells (8.88%), which continued to increase by day 4, with the total annexin-positive population rising to 47.4% of the population. PARP cleavage was evident by 2 days posttransfection and persisted through day 4 of HEI-C depletion. These results confirm that in an asynchronous population of cells, lack of HEI-C results in the induction of apoptosis and an overall decrease in the G_2/M compartment of the cell cycle.

HEI-C is required for passage through mitosis. The reduced G_2/M compartment and the increased degree of apoptosis identified in asynchronous cells with depleted HEI-C may represent linked phenomena, in which HEI-C-depleted cells are specifically unable to complete G_2/M and apoptose. Alternatively, it might reflect two separable outcomes, in which HEI-C could be inducing apoptosis regardless of cell cycle compartment and also inducing arrest at an earlier stage in cell division, yielding an overall decrease in the number of cells able to enter G_2/M . To determine which of these hypotheses was correct, HEI-C-depleted cells were synchronized by treatment with hydroxyurea in G_1/S phase. Cells were released into the cell cycle and monitored by FACS, videomicroscopy, and immunofluorescence. FACS analysis (Fig. 6A) indicated that HEI-C-depleted cells synchronized effectively following hydroxyurea block and emerged from hydroxyurea block and proceeded through S and G_2 with efficiency and kinetics similar to those in control cells.

In contrast, a drastic difference between HEI-C-depleted cells and controls was observed in mitosis. As the cells reached mitosis at 10 h postrelease (confirmed by simultaneous immunofluorescence), the number of cells progressing through the cell cycle diminished by 90% and the predominant material in the sample was debris (results shown are representative of



three independent experiments). These results revealed a crisis in mitosis for HEI-C-depleted cells. In addition, lysates collected from the synchronized and released cells were probed for PARP cleavage as a gauge of apoptosis (Fig. 6B). p85 PARP was present in all fractions. Although the ratio of cleaved to uncleaved PARP appeared somewhat elevated in the mitotic fraction (Fig. 6B, far right lane), it was difficult to draw a firm conclusion because the consistent gross reduction in intact cells (Fig. 6A, bottom right) limited the material for analysis. In sum, our data indicate that although HEI-C-depleted cells clearly have some markers of apoptosis, the crisis and disintegration of the cells are critically linked to passage through mitosis and potentially involve nonapoptotic mechanisms.

HEI-C depletion induces aberrant spindle morphology and cellular demise during the metaphase-anaphase transition.

We used video microscopy to analyze HEI-C-depleted or control transfected cells released from hydroxyurea block (observation beginning 6 h postrelease). The intervals from cell rounding to metaphase plate formation (R to M), metaphase to anaphase (M to A), anaphase to cleavage furrow formation (A to CF), and cleavage furrow formation to cytokinesis (CF to C) were recorded (Table 1). The interval between cell rounding and metaphase plate formation was 26 min for transfection control cells, compared to 49 min for HEI-C.A-ransfected cells, reflecting a moderate delay. A more dramatic difference was seen in the HEI-C-depleted cells versus control cells at the metaphase-anaphase interval. In control transfected cells this interval was 30 min, while the HEI-C-depleted cells that completed this interval required 141 min. However, many (46%) of the HEI-C-depleted cells did not successfully complete mitosis at all.

We distinguished two distinct classes of mitotic defects among the HEI-C-depleted cells (Fig. 7). Class I cells experienced a delay between metaphase plate formation and anaphase, with no delays in anaphase to cleavage furrow formation or completion of cytokinesis. In contrast, class II experienced catastrophic cell disintegration or explosion after metaphase plate formation. The class II cells appeared to form a metaphase plate appropriately, yet in some cells the metaphase plate was seen to move as if being pulled and finally to dissolve. After the metaphase plate was no longer visible these cells disintegrated, although the timing of this interval to explosion varied greatly, from minutes to many hours. It is this class of cells that is likely to represent the debris fraction in the FACS analysis and the loss of G₂/M in the asynchronous steady-state population. Of 28 scored cells initiating mitosis, 3 cells transitioned through mitosis normally, 12 completed mitosis

with a significant delay (class I), and 13 disintegrated (class II). It is important to note that the fate of the progeny of class I cells is unknown. Although a small portion died during the time of observation, it is possible that all progeny of these mitoses are nonviable.

Parallel confocal analysis of HEI-C-depleted samples costained for tubulin (Fig. 8A and C, panels a to f, in red) and DNA (Fig. 8 panels B and C, panels a to f, in blue) indicated that depletion of HEI-C resulted in aberrant spindle morphology compared to controls (Fig. 8A, B, and C, panels g and h). The images provided represent a range of severity of the observed defects. In some cases (Fig. 8A, panel a), spindles showed few differences from the spindles found in wild-type cells. However, in many cases, the aberrant spindles were smaller or asymmetrical or showed less intense microtubule staining than those in control cells. In some cases, multipolar spindles were clearly apparent (e.g., Fig. 8A, panels e and f), although not all the supernumerary spindles appeared to be functional, based on the orientation of the DNA in these cells (Fig. 8B and C, panels e and f). Further inspection of the DNA in HEI-C-depleted cells in some cases suggested that chromatin compaction was reduced relative to controls (Fig. 8B, panels c and d). Some cells were clearly destined for disintegration (i.e., presumed to be class II), as DNA fragments were visible (not shown). We note that the cells available for analysis by immunofluorescence are unlikely to represent the cells with the most extreme mitotic defects, based on the analysis of videomicroscopy data presented above, as the cells which have the most dramatic mitotic defects are frequently floating or disintegrate rapidly, precluding quantitative analysis of this population by immunofluorescence.

To determine if the spindle defects observed by confocal microscopy were caused by inefficient focusing of microtubule minus ends at spindle poles, we used the previously described *in vitro* assay of microtubule aster assembly (see above). Affinity-purified anti-HEI-C antibodies or control preimmune antibodies were used to deplete HEI-C protein from HeLa cell mitotic extracts prior to stimulating aster assembly. Immunodepletion with anti-HEI-C antibodies resulted in depletion of $\approx 95\%$ of HEI-C (Fig. 9A). However, depletion with either control preimmune antibody or anti-HEI-C antibody had no detectable effect on the morphology of mitotic asters (Fig. 9B), the efficiency with which asters formed, or the presence of other known aster components such as NuMA. These results indicate that microtubule focusing at poles does not require HEI-C and suggest that the mitotic defects observed by con-

FIG. 5. Decrease in G₂/M compartment of the cell cycle is accompanied by the appearance of a sub-G₁ population in HEI-C-depleted cells. (A) Western analysis of siRNA-transfected cells. HeLa cells were untreated (U), treated with transfection reagent alone (M), transfected with a control siRNA (C), or transfected with a siRNA directed against HEI-C, HEI-C.A (A). Cell lysates were subjected to electrophoresis, transferred to a polyvinylidene difluoride membrane, probed with antibody to HEI-C antibodies, and subsequently stripped and reprobbed with actin as a loading control. (B) HeLa cells that were untreated, transfected with a control siRNA, or transfected with the HEI-C.A siRNA were harvested at the indicated number of days (d) after siRNA transfection and fixed at -20°C in 70% ethanol. The cells were subsequently stained with propidium iodide and analyzed by FACSscan. (C) HeLa cells were either left untreated or transfected with either a control siRNA or the HEI-C-directed siRNA HEI-C.A and analyzed simultaneously for live annexin and propidium iodide staining at the times indicated after transfection by FACSscan. Cell populations were analyzed with FlowJo software. The percent annexin-positive cells is shown. (D) Western analysis of HeLa cells untreated (U), transfected with a control siRNA (C), or transfected with the HEI-C-directed siRNA HEI-C.A (A). Cells were lysed in RIPA buffer, subjected to electrophoresis on an SDS-10% PAGE gel, transferred to a polyvinylidene difluoride membrane, and immunoblotted with anti-p85 PARP antibodies.

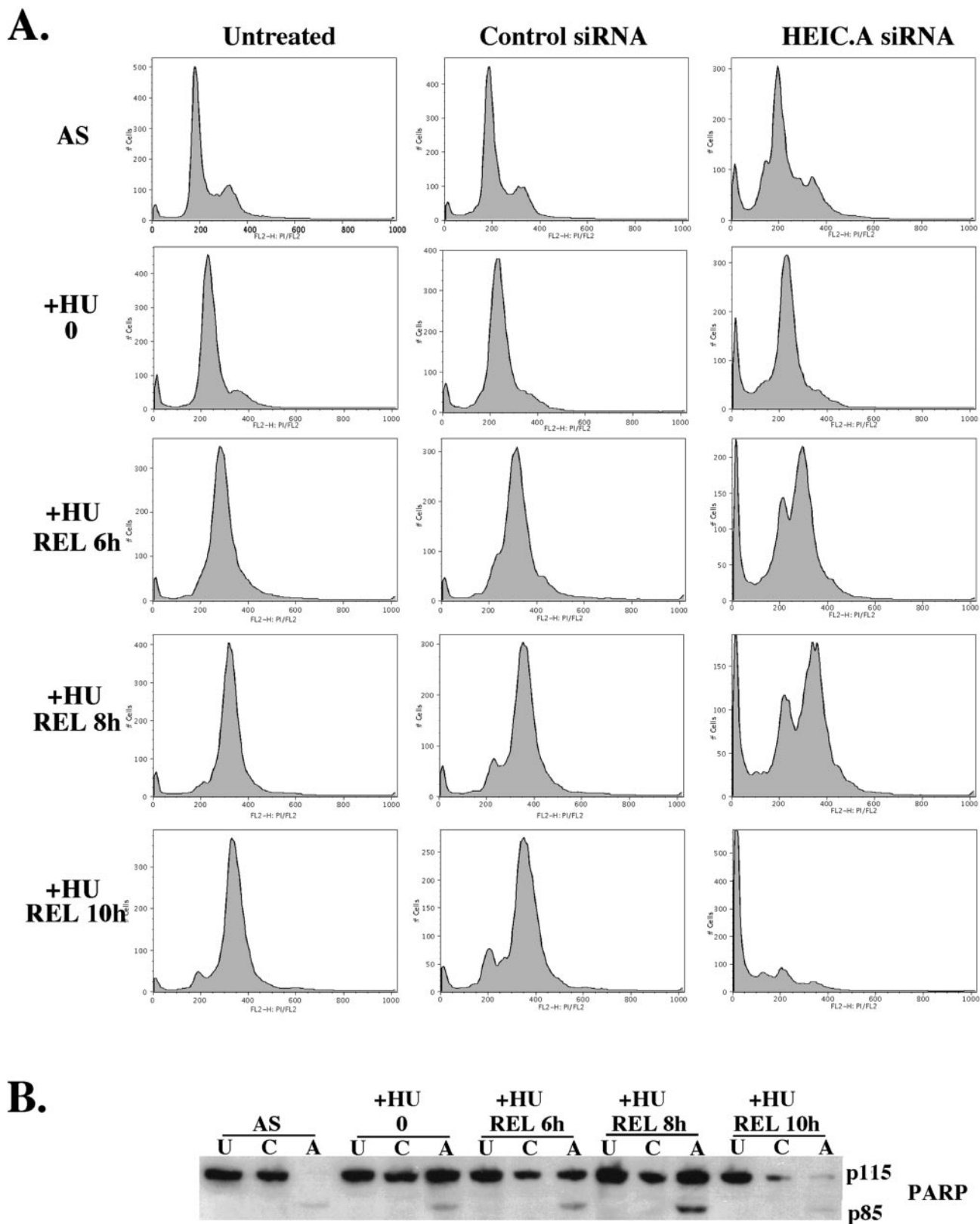


FIG. 6. HEI-C is required for passage through mitosis. (A) HeLa cells were either left untreated, transfected with a control siRNA, or transfected with the HEIC.A siRNA for 72 h. The cells were either allowed to continue untreated (asynchronous, AS) or treated with hydroxyurea for 20 h prior to harvest (i.e., at 52 h following siRNA transfection) to block cell cycle progression (+HU, 0) or treated with hydroxyurea, and then washed free of drug and released to enter the cell cycle for the indicated number of hours (6, 8, or 10 h postrelease [REL]). Cells were harvested and fixed at -20°C in 70% ethanol. The cells were subsequently stained with propidium iodide and analyzed by FACSscan. (B) Western analysis of HeLa cells untreated (U), transfected with a control siRNA (C), or transfected with the HEIC-directed siRNA, HEIC.A (A). Cells were lysed in RIPA buffer, subjected to electrophoresis on an SDS-10% PAGE gel, transferred to a polyvinylidene difluoride membrane, and immunoblotted with affinity-purified rabbit polyclonal anti-PARP antibodies.

TABLE 1. Quantitation of cell cycle progression in HEI-C-depleted cells

Cells tested	Mean. no. of cells (SD) at interval ^a :			
	R to M	M to A	A to CF	CF to C
Control (<i>n</i> = 19)	26 (13)	30 (12)	7 (3)	8 (2.4)
HEI.C.A transfected (<i>n</i> = 27)	53 (37.14)	141.4 (110)	12.8 (11.73)	19.73 (20.4)

^a Intervals tested were from cell rounding to metaphase plate formation (R to M), metaphase to anaphase (M to A), anaphase to cleavage furrow formation (A to CF), and cleavage furrow formation to cytokinesis (CF to C).

focal and video microscopy in cells lacking HEI-C reflect defects in mitotic regulation independent of mitotic spindle pole organization.

Finally, mitotic checkpoint controls serve to preserve cell viability in the face of mitotic defects. The fact that HEI-C-depleted cells died in mitosis raises the possibility that HEI-C depletion may affect checkpoint signaling. To determine if cells depleted of HEI-C have an intact spindle checkpoint, HEI-C-depleted cells were treated with nocodazole to assess if these cells retained the ability to activate the spindle checkpoint. Cells depleted of HEI-C and transfected with a control siRNA or left untreated were treated with nocodazole, and the cells were analyzed by FACS analysis. HEI-C-depleted cells clearly had an intact spindle checkpoint (Fig. 9C), as indicated by their efficient synchronization at G₂/M.

DISCUSSION

The results presented above indicate an essential function for HEI-C in progression through mitosis. The localization of HEI-C to the mitotic asters, the association of the protein with

a high-molecular-weight complex in mitotic lysates, and the severe defects in spindle function accompanied by cell death in HEI-C-depleted cells together indicate that one important element of HEI-C activity is regulation of the mitotic spindle. Biochemical studies exclude the possibility that HEI-C depletion directly affects mitotic aster formation or recruitment of several other aster-associated proteins. This groups HEI-C with a number of proteins with a known role at the spindle that also do not affect aster formation in vitro, including CLIP-170 (13), TPX2 (21), and MCAK and KIF4 (47).

For the other proteins studied, it is becoming appreciated that their lack of a scorable in vitro phenotype reflects a role in control of spindle architecture in the specific context of a bipolar spindle, and HEI-C may function similarly. However, HEI-C does not conform to any previously identified class of proteins that are known to regulate the mitotic spindle. Its sequence does not predict an enzymatic activity, precluding it from two major groups of spindle regulators, kinases and motors, nor does HEI-C contain consensus sequences for phosphorylation by known cell cycle-regulatory kinases. Based on

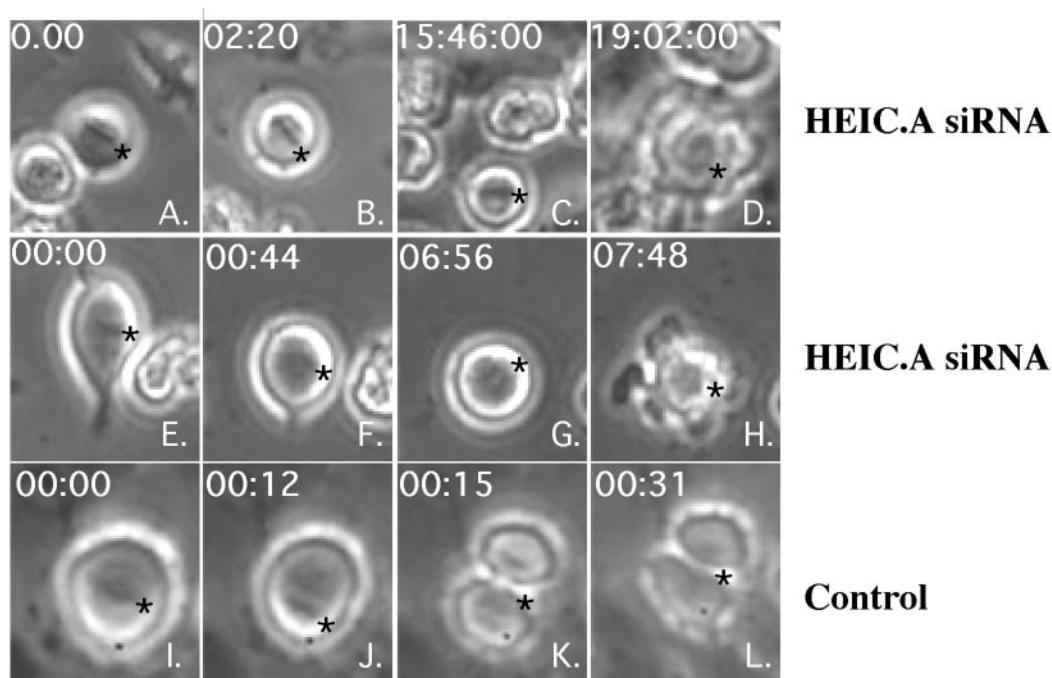


FIG. 7. Video microscopy of HEI-C-depleted cells in mitosis. HeLa cells were either transfected with the HEI.C.A siRNA (panels A to H) or transfected with a control siRNA (panels I to L) for 72 h. 20 h prior to assessment, cells were treated with hydroxyurea to block cell cycle progression, then washed free of drug, and allowed to enter the cell cycle to enrich for cells in M phase. The first frame corresponds to the first appearance of a metaphase plate, while the times shown on each frame indicate time since the first frame. Asterisks mark cells tracked for the indicated time intervals.

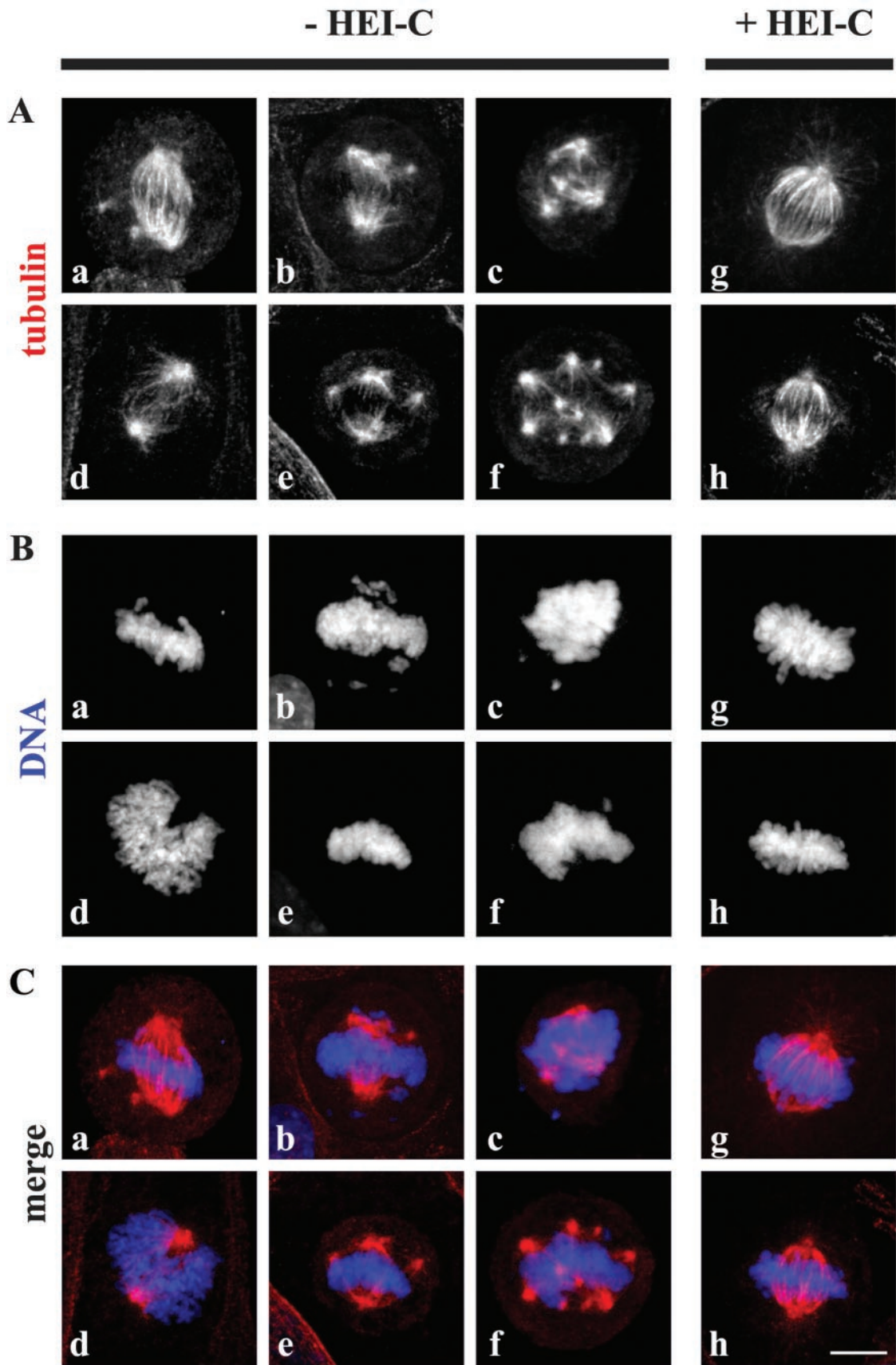


FIG. 8. Confocal analysis of HEI-C-depleted cells. HeLa cells that were depleted of HEI-C.A (a to f) versus nondepleted controls (g and h) were fixed in 4% paraformaldehyde and costained with antitubulin antibodies (A) and SYTOX-Green nucleic acid stain (B). (C) Merged images of tubulin in red and DNA in blue. Bar, 10 μ m.

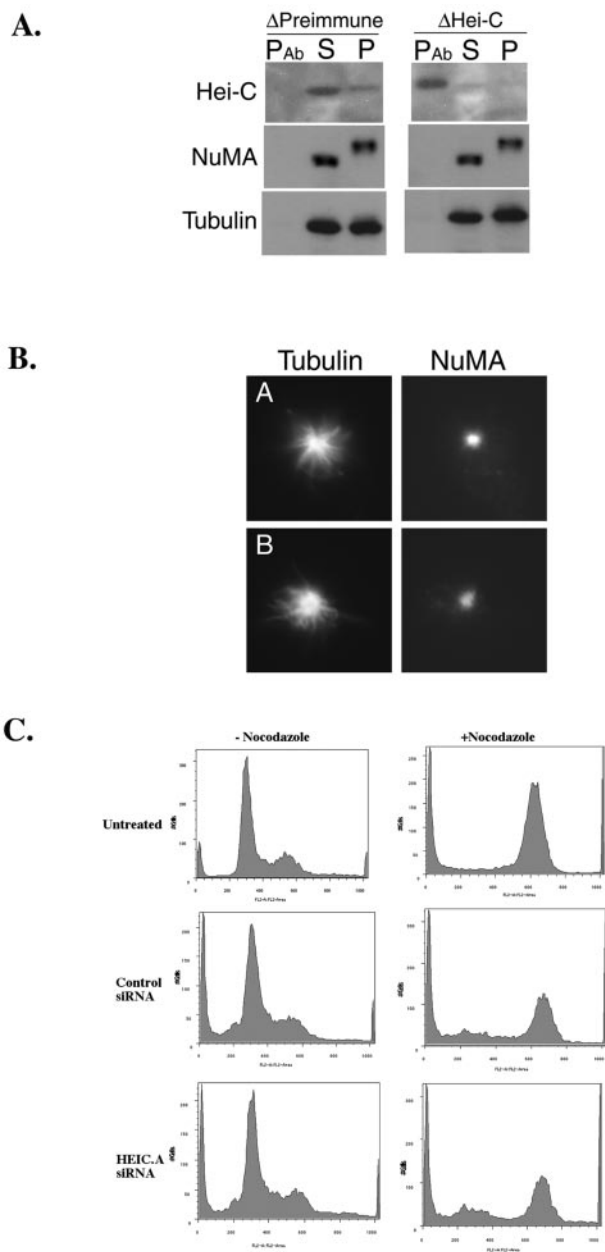


FIG. 9. HEI-C is not required for spindle assembly, and HEI-C depletion does not impair the spindle checkpoint. (A) HeLa cell mitotic extract was immunodepleted with protein A-conjugated agarose containing immunoglobulin G from the preimmune rabbit serum (A) or protein A-conjugated agarose containing affinity-purified antibodies against HEI-C (B). The protein A-conjugated agarose was recovered (PAb) from the depletion steps, and the remainder of the extracts was separated into soluble (S) and insoluble (P) fractions following aster assembly by centrifugation at $10,000 \times g$. These fractions were subjected to Western analysis (D) with antibodies to HEI-C, NuMA, and tubulin as indicated. (B) Following depletion as described for A., microtubule asters were assembled under standard conditions with taxol and ATP for 30 to 60 min at 30°C and processed for indirect immunofluorescence (A and B) with α -tubulin- and NuMA-specific antibodies as indicated. (C) HEI-C-depleted cells have an intact spindle checkpoint. HeLa cells were either untreated, transfected with a control siRNA, or transfected with the HEI-C siRNA for 48 h, then treated with nocodazole (+nocodazole) for 14 h or left untreated (-nocodazole). Cells were harvested by fixation at -20°C in 70% ethanol. The cells were subsequently stained with propidium iodide and analyzed by FACScan.

this profile, and based on the extensively coiled-coiled nature of HEI-C, we predict that HEI-C is a previously unidentified element of a complex involved in regulation of spindle integrity and functionality from metaphase through anaphase.

Based on the analysis of the consequences of HEI-C depletion, HEI-C is required for successful passage through mitosis. The normal duration of progress from rounding to metaphase indicates that the requirement for HEI-C is not critical in this interval (Table 1). In addition, immunodepletion of HEI-C in an assay for microtubule focusing at spindle poles showed no effect. Our data clearly indicate that lack of HEI-C imposes severe defects following metaphase plate formation, with consequences including metaphase-to-anaphase delay (class I) or cellular disintegration (class II). These observations, coupled with the fact class I cells have no delays in completing mitosis after their eventual entry into anaphase, suggest that HEI-C is required in M phase primarily for the completion of the metaphase-to-anaphase transition.

It is likely that the defects observed by immunofluorescence of HEI-C-depleted cells represent an underestimate of the consequences of the depletion of HEI-C, since many of the abnormal cells were removed from the population. The FACS analysis of HEI-C depletion in asynchronous cells over a time course of 4 days indicates the accumulation of a sub- G_0 population and annexin-positive cells commencing at day 2 (Fig. 5B and C) or within 24 h of the earliest detectable depletion of HEI-C (data not shown). The cells in these populations may partly reflect the death of class II cells that have died in mitosis in the absence of HEI-C, but may additionally include the progeny of class I cells. Based on our analysis showing that some of the class I daughter cells died, a significant fraction of the progeny of these cells is potentially unviable in spite of their success in passage through M phase.

Class II cells undergo disintegration or explosion subsequent to metaphase plate formation. Biochemical markers of apoptosis are present, indicating that the mechanism of cell death may share some characteristics with classical apoptosis. However, in synchronized HEI-C-depleted cells, the amount of cleaved PARP did not increase specifically during mitosis, indicating that the cell disintegration seen during videomicroscopy may not be classical apoptosis, but rather mitotic catastrophe (4, 50, 67). Further supporting this idea, given that HEI-C-depleted cells are often characterized by aberrant and misaligned spindles, these cells would be predicted to undergo mitotic arrest as a result of spindle checkpoint activation and hence protected from apoptosis (22, 30, 64, 75). The fact that HEI-C-depleted cells are capable of arresting in response to nocodazole treatment (Fig. 8E) implies that a spindle checkpoint is intact; hence, the high frequency of cellular rupture observed at the metaphase-to-anaphase transition in these cells is extremely unusual. A limited number of reports have described cell death in this metaphase-to-anaphase compartment in response to loss of mitotic regulatory proteins, including, for example, a recent description of the consequences of depletion of the kinetochore-associated protein hNuf2 (10). However, cell death associated with hNuf2 depletion is marked by blebbing and formation of membrane protrusions, while cells depleted of HEI-C appear morphologically normal by phase microscopy until their sudden rupture. The mechanistic basis for this phenomenon will be an area of future investigations.

The coiled-coil sequence of HEI-C provides few clues as to protein function and has also impeded the use of standard technologies such as the two-hybrid system to identify specific protein interactors that might assign HEI-C to a defined regulatory pathway (data not shown). The fact that HEI-C is found in a high-molecular-weight complex at mitosis (Fig. 4B) is compatible with its association with other spindle-associated proteins. It is interesting that HEI-C was identified in a cross-species functional screen involving *S. cerevisiae*. Coiled-coil proteins that are involved in regulation of the mitotic spindle and cell death in higher eukaryotes in some cases have orthologs in *S. cerevisiae*, and mutations in these orthologs can induce abnormal budding. Coiled-coil domains are prevalent in spindle-associated motor proteins (e.g., dynein) (20) and other spindle-associated regulatory factors, e.g., the checkpoint protein Mad1 (25) and survivin (41), and the integrity of these coiled-coil domains has been shown to be important for protein function (41, 65).

There are particularly suggestive parallels between the activity of HEI-C as defined herein and the activity of survivin. Inhibitor of apoptosis (IAP) proteins, which include survivin, were first defined as a group of viral proteins that blocked cell defenses by eliminating their ability to undergo cell death. Depletion of survivin function by antisense RNA or by knock-out results in aberrant spindle formation and polyploidy (6, 30, 41, 56, 73). *BIR* domain proteins are evolutionarily conserved through *C. elegans* and the yeasts, with the detected orthologs most closely related to survivin (18, 41, 46, 72, 73). In the yeasts *S. cerevisiae* and *Schizosaccharomyces pombe*, mutation of *BIR1/bir1* causes mitotic deficiencies similar to those found in higher eukaryotes. These include arrest at the metaphase-to-anaphase transition based on failure to elongate the mitotic spindle; and strikingly, for *S. cerevisiae*, a change in budding profile that has been variously described as unusual cellular elongation (42) and induced pseudohyphal budding (72). These commonalities between survivin and HEI-C in *S. cerevisiae* and higher eukaryotes suggest that HEI-C may be affecting a similar subset of pathways.

Last, although we have clearly defined a role for HEI-C in mitotic progression, an intriguing possibility raised by the complex localization profile of the protein is that HEI-C has additional cellular functions. The observation that HEI-C is additionally enriched at areas of cell-cell contact raises the possibility that HEI-C is involved in transmission of information between the spindle and the cell periphery. This additional localization profile may account for the Northern blot-based predicted abundant expression of HEI-C in differentiated tissues. A number of proteins which migrate between peripheral cellular structures and the mitotic spindle, including HEF1 (37), zyxin (27), dynein (32, 43; reviewed in reference 31), EB1 (reviewed in reference 70), and others have been identified. As noted above, HEF1 was also identified in our laboratory in a screen for human genes which enhance filamentation in *S. cerevisiae*, functions at focal adhesions to provide attachment-induced survival signaling in interphase cells (34, 37), and is required for passage through mitosis (D. Dadke, E. Pugacheva, and E. Golemis, unpublished results). As another example, dynein is required *in vivo* and *in vitro* for spindle formation in mitosis (31), while during interphase it is involved in vesicle trafficking (31) and assembly of adherens junctions (32, 43).

The importance of pathways which coordinate events of the

cell cycle and events at the cell periphery in *S. cerevisiae* has been well established (40), and such pathways are certain to be equally if not more important in higher eukaryotes. Involvement of HEI-C in such coordinating pathways will be a point of future interest.

ACKNOWLEDGMENTS

We thank Joanne Estojak and Ying Tong Wang for excellent technical assistance. We gratefully acknowledge Vicki Mountain for technical assistance with the sucrose gradient fractionation. We thank Jonathan Boyd of the Fox Chase Cancer Center Cell Imaging Facility for assistance with microscopy and Sophie Cotteret for assistance with FACS experiments. We thank Chris Elsasser and John Moeller from the Fox Chase Cancer Center instrumentation shop for constructing a contained environmental stage for live cell microscopy. We thank Sylvie Vincent for the gift of the PRK2 plasmids. We thank Elizabeth Henske and Maureen Murphy for comments on the manuscript. We thank Tim Yen for helpful discussion.

This work was supported by grants from the National Institutes of Health to E.A.G. (CA80991) and to D.A.C. (GM51542), by an NIH Core Grant to Fox Chase Cancer Center, and by Tobacco Settlement funding from the State of Pennsylvania (to E.C.).

REFERENCES

- Amon, A. 1999. The spindle checkpoint. *Curr. Opin. Genet. Dev.* **9**:69–75.
- Barral, Y., S. Jentsch, and C. Mann. 1995. G₁ cyclin turnover and nutrient uptake are controlled by a common pathway in yeast. *Genes Dev.* **9**:399–409.
- Braverman, L. E., and L. A. Quilliam. 1999. Identification of Grb4/Nckbeta, a src homology 2 and 3 domain-containing adapter protein having similar binding and biological properties to Nck. *J. Biol. Chem.* **274**:5542–5549.
- Burns, T. F., P. Fei, K. A. Scata, D. T. Dicker, and W. S. El-Deiry. 2003. Silencing of the novel p53 target gene Snk/Plk2 leads to mitotic catastrophe in paclitaxel (taxol)-exposed cells. *Mol. Cell. Biol.* **23**:5556–5571.
- Chan, G. K., and T. J. Yen. 2003. The mitotic checkpoint: a signaling pathway that allows a single unattached kinetochore to inhibit mitotic exit. *Prog. Cell Cycle Res.* **5**:431–439.
- Chen, J., W. Wu, S. K. Tahir, P. E. Kroeger, S. H. Rosenberg, L. M. Cowser, F. Bennett, S. Krajewski, M. Krajewska, K. Welsh, J. C. Reed, and S. C. Ng. 2000. Down-regulation of survivin by antisense oligonucleotides increases apoptosis, inhibits cytokinesis and anchorage-independent growth. *Neoplasia* **2**:235–241.
- Clodi, K., K. O. Kliche, S. Zhao, D. Weidner, T. Schenk, U. Consoli, S. Jiang, V. Snell, and M. Andreeff. 2000. Cell-surface exposure of phosphatidylserine correlates with the stage of fludarabine-induced apoptosis in chronic lymphocytic leukemia and expression of apoptosis-regulating genes. *Cytometry* **40**:19–25.
- Compton, D. A. 1998. Production of M-phase and I-phase extracts from mammalian cells. *Methods Enzymol.* **298**:331–339.
- Compton, D. A. 2000. Spindle assembly in animal cells. *Annu. Rev. Biochem.* **69**:95–114.
- DeLuca, J. G., B. Moree, J. M. Hickey, J. V. Kilmartin, and E. D. Salmon. 2002. hNuf2 inhibition blocks stable kinetochore-microtubule attachment and induces mitotic cell death in HeLa cells. *J. Cell Biol.* **159**:549–555.
- den Elzen, N., and J. Pines. 2001. Cyclin A is destroyed in prometaphase and can delay chromosome alignment and anaphase. *J. Cell Biol.* **153**:121–136.
- Drubin, D. G., and W. J. Nelson. 1996. Origins of cell polarity. *Cell* **84**:335–344.
- Dujardin, D., U. I. Wacker, A. Moreau, T. A. Schroer, J. E. Rickard, and J. R. De Mey. 1998. Evidence for a role of CLIP-170 in the establishment of metaphase chromosome alignment. *J. Cell Biol.* **141**:849–862.
- Elbashir, S. M., W. Lendeckel, and T. Tuschl. 2001. RNA interference is mediated by 21- and 22-nucleotide RNAs. *Genes Dev.* **15**:188–200.
- Fashena, S. J., M. B. Einarson, G. M. O'Neill, C. P. Patriotis, and E. A. Golemis. 2002. Dissection of HEF1-dependent functions in motility and transcriptional regulation. *J. Cell Sci.* **115**:99–111.
- Flynn, P., H. Mellor, R. Palmer, G. Panayotou, and P. J. Parker. 1998. Multiple interactions of PRK1 with RhoA. Functional assignment of the Hrl repeat motif. *J. Biol. Chem.* **273**:2698–2705.
- Fornierod, M., M. Ohno, M. Yoshida, and I. W. Mattaj. 1997. CRM1 is an export receptor for leucine-rich nuclear export signals. *Cell* **90**:1051–1060.
- Fraser, A. G., C. James, G. I. Evan, and M. O. Hengartner. 1999. *Caenorhabditis elegans* inhibitor of apoptosis protein (IAP) homologue BIR-1 plays a conserved role in cytokinesis. *Curr. Biol.* **9**:292–301.
- Gaglio, T., A. Saredi, and D. A. Compton. 1995. NuMA is required for the organization of microtubules into aster-like mitotic arrays. *J. Cell Biol.* **131**:693–708.
- Garber, A. T., J. D. Retief, and G. H. Dixon. 1989. Isolation of dynein heavy

- chain cDNAs from trout testis which predict an extensive carboxyl-terminal alpha-helical coiled-coil domain. *EMBO J.* **8**:1727-1734.
21. **Garrett, S., K. Auer, D. A. Compton, and T. M. Kapoor.** 2002. hTPX2 is required for normal spindle morphology and centrosome integrity during vertebrate cell division. *Curr. Biol.* **12**:2055-2059.
 22. **Gillett, E. S., and P. K. Sorger.** 2001. Tracing the pathway of spindle assembly checkpoint signaling. *Dev. Cell* **1**:162-164.
 23. **Gimeno, C. J., P. O. Ljungdahl, C. A. Styles, and G. R. Fink.** 1992. Unipolar cell divisions in the yeast *S. cerevisiae* lead to filamentous growth: regulation by starvation and RAS. *Cell* **68**:1077-1090.
 24. **Hagting, A., N. Den Elzen, H. C. Vodermaier, I. C. Waizenegger, J. M. Peters, and J. Pines.** 2002. Human securin proteolysis is controlled by the spindle checkpoint and reveals when the APC/C switches from activation by Cdc20 to Cdh1. *J. Cell Biol.* **157**:1125-1137.
 25. **Hardwick, K. G., and A. W. Murray.** 1995. Mad1p, a phosphoprotein component of the spindle assembly checkpoint in budding yeast. *J. Cell Biol.* **131**:709-720.
 26. **Herbert, M., M. Levasseur, H. Homer, K. Yallop, A. Murdoch, and A. McDougall.** 2003. Homologue disjunction in mouse oocytes requires proteolysis of securin and cyclin B1. *Nat. Cell Biol.* **5**:1023-1025.
 27. **Hirota, T., T. Morisaki, Y. Nishiyama, T. Marumoto, K. Tada, T. Hara, N. Masuko, M. Inagaki, K. Hatakeyama, and H. Saya.** 2000. Zyxin, a regulator of actin filament assembly, targets the mitotic apparatus by interacting with h-warts/LATS1 tumor suppressor. *J. Cell Biol.* **149**:1073-1086.
 28. **Hood, J. K., and P. A. Silver.** 2000. Diverse nuclear transport pathways regulate cell proliferation and oncogenesis. *Biochim. Biophys. Acta* **1471**:31-41.
 29. **Hoyt, M. A.** 2001. A new view of the spindle checkpoint. *J. Cell Biol.* **154**:909-911.
 30. **Kaitna, S., M. Mendoza, V. Jantsch-Plunger, and M. Glotzer.** 2000. Incentp and an aurora-like kinase form a complex essential for chromosome segregation and efficient completion of cytokinesis. *Curr. Biol.* **10**:1172-1181.
 31. **Karki, S., and E. L. Holzbaur.** 1999. Cytoplasmic dynein and dynactin in cell division and intracellular transport. *Curr. Opin. Cell Biol.* **11**:45-53.
 32. **Karki, S., L. A. Ligon, J. DeSantis, M. Tokito, and E. L. Holzbaur.** 2002. PLAC-24 is a cytoplasmic dynein-binding protein that is recruited to sites of cell-cell contact. *Mol. Biol. Cell* **13**:1722-1734.
 33. **Kron, S. J., and N. A. Gow.** 1995. Budding yeast morphogenesis: signalling, cytoskeleton and cell cycle. *Curr. Opin. Cell Biol.* **7**:845-855.
 34. **Law, S. F., J. Estojak, B. Wang, T. Mysliwiec, G. Kruh, and E. A. Golemis.** 1996. Human enhancer of filamentation 1, a novel p130^{cas}-like docking protein, associates with focal adhesion kinase and induces pseudohyphal growth in *Saccharomyces cerevisiae*. *Mol. Cell Biol.* **16**:3327-3337.
 35. **Law, S. F., G. M. O'Neill, S. J. Fashena, M. B. Einarson, and E. A. Golemis.** 2000. The docking protein HEF1 is an apoptotic mediator at focal adhesion sites. *Mol. Cell Biol.* **20**:5184-5195.
 36. **Law, S. F., Y.-Z. Zhang, S. Fashena, G. Toby, J. Estojak, and E. A. Golemis.** 1999. Dimerization of the docking/adaptor protein HEF1 via a carboxy-terminal helix-loop-helix domain. *Exp. Cell Res.* **252**:224-235.
 37. **Law, S. F., Y.-Z. Zhang, A. Klein-Szanto, and E. A. Golemis.** 1998. Cell-cycle regulated processing of HEF1 to multiple protein forms differentially targeted to multiple compartments. *Mol. Cell Biol.* **18**:3540-3551.
 38. **Leopold, P., and P. H. O'Farrell.** 1991. An evolutionarily conserved cyclin homolog from drosophila rescues yeast deficient in G1 cyclins. *Cell* **66**:1207-1216.
 39. **Lew, D. J., V. Dulic, and S. I. Reed.** 1991. Isolation of three novel human cyclins by rescue of G1 cyclin (Cln) function in yeast. *Cell* **66**:1197-1206.
 40. **Lew, D. J., and S. I. Reed.** 1993. Morphogenesis in the yeast cell cycle: regulation by Cdc28 and cyclins. *J. Cell Biol.* **120**:1305-1320.
 41. **Li, F., G. Ambrosini, E. Y. Chu, J. Plescia, S. Tognin, P. C. Marchisio, and D. C. Altieri.** 1998. Control of apoptosis and mitotic spindle checkpoint by survivin. *Nature* **396**:580-584.
 42. **Li, F., P. L. Flanary, D. C. Altieri, and H. G. Dohlman.** 2000. Cell division regulation by BIR1, a member of the inhibitor of apoptosis family in yeast. *J. Biol. Chem.* **275**:6707-6711.
 43. **Ligon, L. A., S. Karki, M. Tokito, and E. L. Holzbaur.** 2001. Dynein binds to beta-catenin and may tether microtubules at adherens junctions. *Nat. Cell Biol.* **3**:913-917.
 44. **Liu, H., C. A. Styles, and G. R. Fink.** 1993. Elements of the yeast pheromone response pathway required for filamentous growth of diploids. *Science* **262**:1741-1744.
 45. **Liu, H., C. A. Styles, and G. R. Fink.** 1996. *Saccharomyces cerevisiae* S288C has a mutation in FLO8, a gene required for filamentous growth. *Genetics* **144**:967-978.
 46. **Lupas, A., M. Van Dyke, and J. Stock.** 1991. Predicting coiled coils from protein sequences. *Science* **252**:1162-1164.
 47. **Mack, G. J., and D. A. Compton.** 2001. Analysis of mitotic microtubule-associated proteins using mass spectrometry identifies astrin, a spindle-associated protein. *Proc. Natl. Acad. Sci. USA* **98**:14434-14439.
 48. **Makalowski, W., and M. S. Boguski.** 1998. Evolutionary parameters of the transcribed mammalian genome: an analysis of 2,820 orthologous rodent and human sequences. *Proc. Natl. Acad. Sci. USA* **95**:9407-9412.
 49. **Meyer, B. E., and M. H. Malim.** 1994. The HIV-1 Rev trans-activator shuttles between the nucleus and the cytoplasm. *Genes Dev.* **8**:1538-1547.
 50. **Mikhailov, A., R. W. Cole, and C. L. Rieder.** 2002. DNA damage during mitosis in human cells delays the metaphase/anaphase transition via the spindle-assembly checkpoint. *Curr. Biol.* **12**:1797-1806.
 51. **Mosch, H. U.** 2000. Pseudohyphal development of *Saccharomyces cerevisiae*. *Contrib. Microbiol.* **5**:185-200.
 52. **Murray, A. W., M. J. Solomon, and J. W. Kirschner.** 1989. The role of cyclin synthesis and degradation in the control of maturation promoting factor activity. *Nature.* **339**:280-286.
 53. **O'Connell, C. B., and Y. L. Wang.** 2000. Mammalian spindle orientation and position respond to changes in cell shape in a dynein-dependent fashion. *Mol. Biol. Cell* **11**:1765-1774.
 54. **Olie, R. A., A. P. Simoes-Wüst, B. Baumann, S. H. Leech, D. Fabbro, R. A. Stahel, and U. Zangemeister-Wittke.** 2000. A novel antisense oligonucleotide targeting survivin expression induces apoptosis and sensitizes lung cancer cells to chemotherapy. *Cancer Res.* **60**:2805-2809.
 55. **O'Neill, G. M., S. J. Fashena, and E. A. Golemis.** 2000. Integrin signaling: a new Cas(t) of characters enters the stage. *Trends Cell Biol.* **10**:111-119.
 56. **O'Neill, G. M., and E. A. Golemis.** 2001. Proteolysis of the docking protein HEF1 and implications for focal adhesion dynamics. *Mol. Cell Biol.* **21**:5094-5108.
 57. **Palmer, R. H., J. Ridden, and P. J. Parker.** 1995. Cloning and expression patterns of two members of a novel protein-kinase-C-related kinase family. *Eur. J. Biochem.* **227**:344-351.
 58. **Pan, X., and J. Heitman.** 1999. Cyclic AMP-dependent protein kinase regulates pseudohyphal differentiation in *Saccharomyces cerevisiae*. *Mol. Cell Biol.* **19**:4874-4887.
 59. **Quilliam, L. A., Q. T. Lambert, L. A. Mickelson-Young, J. K. Westwick, A. B. Sparks, B. K. Kay, N. A. Jenkins, D. J. Gilbert, N. G. Copeland, and C. J. Der.** 1996. Isolation of a NCK-associated kinase, PRK2, an SH3-binding protein and potential effector of Rho protein signaling. *J. Biol. Chem.* **271**:28772-28776.
 60. **Roberts, R. L., and G. R. Fink.** 1994. Elements of a single MAP kinase cascade in *Saccharomyces cerevisiae* mediate two developmental programs in the same cell type: mating and invasive growth. *Genes Dev.* **8**:2974-2985.
 61. **Rua, D., B. T. Tobe, and S. J. Kron.** 2001. Cell cycle control of yeast filamentous growth. *Curr. Opin. Microbiol.* **4**:720-727.
 62. **Sampath, D., and W. Plunkett.** 2001. Design of new anticancer therapies targeting cell cycle checkpoint pathways. *Curr. Opin. Oncol.* **13**:484-490.
 63. **Seong, Y. S., K. Kamijo, J. S. Lee, E. Fernandez, R. Kuriyama, T. Miki, and K. S. Lee.** 2002. A spindle checkpoint arrest and a cytokinesis failure by the dominant-negative polo-box domain of Plk1 in U-2 OS cells. *J. Biol. Chem.* **277**:32282-32293.
 64. **Shah, J. V., and D. W. Cleveland.** 2000. Waiting for anaphase: Mad2 and the spindle assembly checkpoint. *Cell* **103**:997-1000.
 65. **Sironi, L., M. Mapelli, S. Knapp, A. De Antoni, K. T. Jeang, and A. Musacchio.** 2002. Crystal structure of the tetrameric Mad1-Mad2 core complex: implications of a 'safety belt' binding mechanism for the spindle checkpoint. *EMBO J.* **21**:2496-2506.
 66. **Stade, K., C. S. Ford, C. Guthrie, and K. Weis.** 1997. Exportin 1 (Crm1p) is an essential nuclear export factor. *Cell* **90**:1041-1050.
 67. **Takada, S., A. Kelkar, and W. E. Theurkauf.** 2003. Drosophila checkpoint kinase 2 couples centrosome function and spindle assembly to genomic integrity. *Cell* **113**:87-99.
 68. **Taylor, W. R., and G. R. Stark.** 2001. Regulation of the G2/M transition by p53. *Oncogene* **20**:1803-1815.
 69. **Thornton, B. R., and D. P. Toczyski.** 2003. Securin and B-cyclin/CDK are the only essential targets of the APC. *Nat. Cell Biol.* **5**:1090-1094.
 70. **Tirnauer, J. S., and B. E. Bierer.** 2000. EBI proteins regulate microtubule dynamics, cell polarity, and chromosome stability. *J. Cell Biol.* **149**:761-766.
 71. **Toby, G. G., W. Gherraby, T. R. Coleman, and E. A. Golemis.** 2003. A novel RING-finger protein, human enhancer of invasion 10 (HEI10), alters mitotic progression through regulation of cyclin B levels. *Mol. Cell Biol.* **23**:2109-2122.
 72. **Uren, A. G., T. Beilharz, M. J. O'Connell, S. J. Bugg, R. van Driel, D. L. Vaux, and T. Lithgow.** 1999. Role for yeast inhibitor of apoptosis (IAP)-like proteins in cell division. *Proc. Natl. Acad. Sci. USA* **96**:10170-10175.
 73. **Uren, A. G., L. Wong, M. Pakusch, K. J. Fowler, F. J. Burrows, D. L. Vaux, and K. H. Choo.** 2000. Survivin and the inner centromere protein INCENP show similar cell-cycle localization and gene knockout phenotype. *Curr. Biol.* **10**:1319-1328.
 74. **Vincent, S., and J. Settleman.** 1997. The PRK2 kinase is a potential effector target of both Rho and Rac GTPases and regulates actin cytoskeletal organization. *Mol. Cell Biol.* **17**:2247-2256.
 75. **Wassmann, K., and R. Benezra.** 2001. Mitotic checkpoints: from yeast to cancer. *Curr. Opin. Genet. Dev.* **11**:83-90.
 76. **Wen, W., J. L. Meinkoth, R. Y. Tsien, and S. S. Taylor.** 1995. Identification of a signal for rapid export of proteins from the nucleus. *Cell* **82**:463-473.
 77. **Yu, H.** 2002. Regulation of APC-Cdc20 by the spindle checkpoint. *Curr. Opin. Cell Biol.* **14**:706-714.